High-power regime of femtosecond-laser pulse propagation in silica: Multiple-cone formation

Kenichi Ishikawa*
Department of Quantum Engineering and Systems Science, Graduate School of Engineering, University of Tokyo, Hongo 7-3-1, Bunkyo-ku, Tokyo 113-8656, Japan

Hiroshi Kumagai and Katsumi Midorikawa
Laser Technology Laboratory, RIKEN (The Institute of Physical and Chemical Research), Hirosawa 2-1, Wako-shi, Saitama 351-0198, Japan

(Received 18 July 2002; published 21 November 2002)

We present a numerical study of the $(2+1)$-dimensional propagation dynamics of femtosecond-laser pulses in silica. In particular, considered are pulses, whose power is tens to hundreds of times higher than the threshold for self-focusing. We solve the axially symmetric, extended, nonlinear Schrödinger equation for the laser electric field, including group velocity dispersion, Kerr nonlinearity, plasma formation and defocusing, self-steepening, and space-time focusing. Our simulation results reveal that the high-power pulses are split spatially, as well as temporally, several times into multiple cones during its propagation. This new structure is formed as a result of the interplay of strong Kerr self-focusing and plasma defocusing. The number of cones and their angle with respect to the propagation axis increase with incident pulse energy. The uncertainty, which may be contained in the evaluation of plasma response and band-to-band transition rate, and the pulse disturbance by modulation instability are also analyzed. Although these influence the details of the pulse propagation, they do not affect the essence of our results: the multiple-cone formation.

DOI: 10.1103/PhysRevE.66.056608 PACS number(s): 42.25.Bs, 42.65.Re, 42.65.Jx, 42.65.Sf

I. INTRODUCTION

The propagation of light in a medium has been fundamental in pure physics as well as important in applied science for centuries. In early days, available light sources were so weak that its propagation was dominated by linear effects. Since the advent of intense femtosecond (fs) laser pulses, complex linear and nonlinear effects originating from their broad spectral bandwidths, short pulse widths, and high peak power have posed significant challenges. For several years, researchers have intensively investigated the propagation of intense fs pulses in gases [1–7], especially in air, and have found various phenomena such as filamentation and pulse splitting. An important parameter is the critical power $P_{cr} = \lambda_0^2/2\pi n_0 n_2$ for self-focusing in the continuous wave limit, where λ_0 denotes the laser wavelength, n_0 the linear refractive index, and n_2 the nonlinear refractive index. The value of P_{cr} is about 3 GW for air at $\lambda_0 = 800$ nm, and work [1–7] for gas has been performed using a power up to a few tens of times P_{cr}. The propagation in solids [8–12] is less studied. Zozulya *et al.* [9] simulated the propagation of fs pulses with a power of 3.9–5.4 MW in the context of multiple splitting, coalescence, and continuum generation. Ranka *et al.* [10] and Tzortzakis *et al.* [11] also studied the propagation of a pulse with a power of several MW and found processes similar to those in a gas. The laser power used in these studies, however, is by orders of magnitude lower than those used in the studies for air. On the other hand, an experiment for silica glass using a power up to 1 GW, several hundred times P_{cr} $(=2.2$ MW), was recently performed [12].

In the present study, we report the results of our numerical simulations of the propagation of cylindrically symmetric Gaussian intense fs-laser pulses in silica. We consider an input pulse power ranging from several tens to several hundreds of times P_{cr}. In such a high-power regime the laser pulse propagation is qualitatively different from that of pulses with a lower power or pulse propagation in gases. After the Kerr self-focusing, the pulse is multiply split in time as well as in space to form multiple cones, which are approximately parallel to each other but not parallel to the propagation axis. The number of the formed cones as well as their angle with respect to the propagation axis increases with the input pulse power. This unique structure originates from a large local variation of the refractive index caused by nonlinear response of silica and plasma formation. The behavior of silica in an intense fs-laser pulse such as the rate of plasma formation and the response of conduction (plasma) electrons has not been sufficiently clarified yet, to the authors' knowledge. The multiple-cone formation, however, seems to be robust against these uncertainties and is also present in cases in which the pulse propagation is disturbed by modulation instability.

The present paper is organized as follows. Section II summarizes the simulation model. In Sec. III, we present the simulation results for ultrashort high-power pulses propagating inside silica. In Sec. III A, we show the evolution of the intensity distribution of the pulse. Upon propagation, especially, the pulse is transformed into a structure made up of several cones. In Sec. III B, we study the mechanism of the formation of these multiple cones. In Secs. III C–III E, we discuss how several uncertainties inherent in the present model affect our simulation results. The conclusions are given in Sec. IV.

*Electronic address: ishiken@q.t.u-tokyo.ac.jp

II. MODEL

Assuming propagation along the z axis, we model the evolution of the complex envelope $E(\mathbf{r},z,t)$ of the electric field $\mathcal{E}(\mathbf{r},z,t)=E(\mathbf{r},z,t)\exp(ik_0z-i\omega_0t)$ with the extended, nonlinear Schrödinger equation [1,4,5,7] in a reference frame moving at the group velocity,

$$\frac{\partial E}{\partial z}+\frac{i}{2}\beta_2\frac{\partial^2 E}{\partial t^2}-\frac{1}{6}\beta_3\frac{\partial^3 E}{\partial t^3}-\frac{i}{2n_0k_0}\left(\frac{\partial^2}{\partial r^2}+\frac{1}{r}\frac{\partial}{\partial r}\right)\times\left(1-\frac{i}{\omega_0}\frac{\partial}{\partial t}\right)E=in_2k_0\left(1+\frac{i}{\omega_0}\frac{\partial}{\partial t}\right)(|E|^2E)-\frac{ik_0}{2}\left(1-\frac{i}{\omega_0}\frac{\partial}{\partial t}\right)\left(\frac{\rho}{\rho_{cr}}E\right)-3\sigma_6(\rho_0-\rho)\left(\frac{|E|^2}{\hbar\omega_0}\right)^5E. \quad (1)$$

E is normalized in such a way that $|E|^2$ gives an intensity in W/cm^2 for convenience, and c denotes the vacuum velocity of light. The second to fourth terms on the left-hand side describe the second- and third-order group velocity dispersion, and transverse diffraction, respectively. The terms on the right-hand side describe the nonlinear Kerr response, the contribution of plasma formation to the refractive index, and loss due to multiphoton absorption. The terms containing an operator $(i/\omega_0)\partial/\partial t$ account for the correction beyond the slowly varying envelope approximation (SVEA) [1,4,8], necessary to treat short pulses considered in the present study.

We choose a laser operating wavelength of $\lambda_0=800$ nm, which corresponds to the angular frequency $\omega_0=2.35$ fs^{-1} and the vacuum wave number $k_0=7.85$ μm^{-1}. The material parameters used in our simulations for silica are as follows: $\beta_2=0.034$ μm^{-1} fs^2, $\beta_3=0.03$ μm^{-1} fs^3, $n_0=1.4533$, $n_2=2.66\times10^{-16}$ cm^2/W. The critical electron density ρ_{cr} for $\lambda_0=800$ nm is 1.74×10^{21} cm^{-3}, and the initial electron density ρ_0 in the valence band is 2.23×10^{22} cm^{-3}. ρ is the density of electrons produced through six-photon band-to-band transitions (the band gap is 9.0 eV). The cross section σ_6 for this process is evaluated to be 2.6×10^{-180} s^5 cm^{12} from the Keldysh theory [13]. Equation (1) is coupled with an equation describing the conduction electron density evolution,

$$\frac{\partial\rho}{\partial t}=\sigma_6\left(\frac{|E|^2}{\hbar\omega_0}\right)^6(\rho_0-\rho). \quad (2)$$

In principle, a term for avalanche ionization should be added to this equation. The classical models [14,15] of optical breakdown, however, cannot be applied in the fs-pulse regime [16,17]. Although several new models [16,17] have been proposed, their validity is yet to be established. On the other hand, no laser-induced damage was observed in the experiments by Kumagai *et al.* [12] under the conditions similar to those in our simulations. Moreover, in our results, the maximum intensity achieved during the propagation is much lower than the threshold for the laser-induced breakdown [18,19] as we will see later in Fig. 2, indicating that multiphoton band-to-band transition dominates plasma formation. We have, therefore, neglected avalanche ionization.

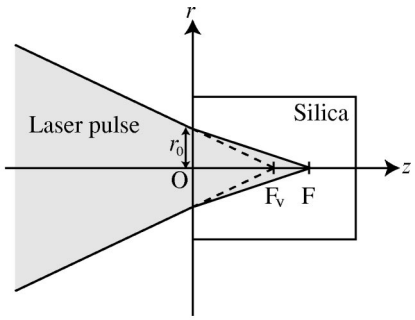

FIG. 1. Schematic of the setup. F, focus in the low-intensity limit ($z=10.9$ mm); F_v, vacuum focus ($z=7.5$ mm). The focused laser pulse is incident onto the silica at $z=0$ from the left along the z axis. The lateral intensity profile at $z=0$ is Gaussian with a FWHM of $2r_0=235.5$ μm. The incident surface is located at $z=2.5$ mm only for the case of Fig. 5.

The loss of electrons due to diffusion and recombination is also negligible in the fs regime [19]. The temporal intensity profile of the incident pulse is proportional to sech^2 with a full width at half maximum (FWHM) of 130 fs. Its lateral profile is Gaussian with a FWHM of 235.5 μm. The geometrical focus is at a propagation distance z of 10.9 mm (Fig. 1). The numerical scheme to solve Eq. (1) is based on the split-step Fourier method [20]. The diffraction term is treated with the method developed by Koonin *et al.* [21], to solve the time-dependent Schrödinger equation in cylindrical coordinates. The nonlinear terms as well as Eq. (2) are integrated using the Runge-Kutta method. In order to prevent reflection of the pulse from the grid boundary, after each time step, we multiply the envelope E of the electric field by a $\cos^{1/8}$ mask function [22] that varies from 1 to 0 over a width of one-eighth of the maximum radius at the outer radial boundary. In fact, as we will see later, virtually no reflection is observed even without this procedure. We have checked the numerical results by doubling the space and time resolution, which led to no visible changes in the behavior of the results presented here. We have also tried a few other schemes to integrate Eq. (1) and confirmed that the results remain virtually the same.

III. RESULTS

A. Evolution of the laser intensity profile

Figure 2 illustrates the spatiotemporal laser intensity profile at different propagation distances z for the input energy of 135 μJ. This translates to the input power $P\approx1$ GW or $4.7\times10^2P_{cr}$. With $z=3200$ μm, the pulse energy is concentrated near the beam axis due to self-focusing, and the peak is shifted toward the trailing edge due to self-steepening [20]. As the self-focusing proceeds and the local intensity increases further, conduction (plasma) electrons are produced through multiphoton absorption. Since the plasma formation has a negative contribution to the refractive index, this leads to defocusing near the trailing edge ($z=3300$ μm) and results in the formation of a conelike structure ($z=3400$ μm). So far, the pulse evolution is similar to those for the input power, which is a few times higher than P_{cr}.

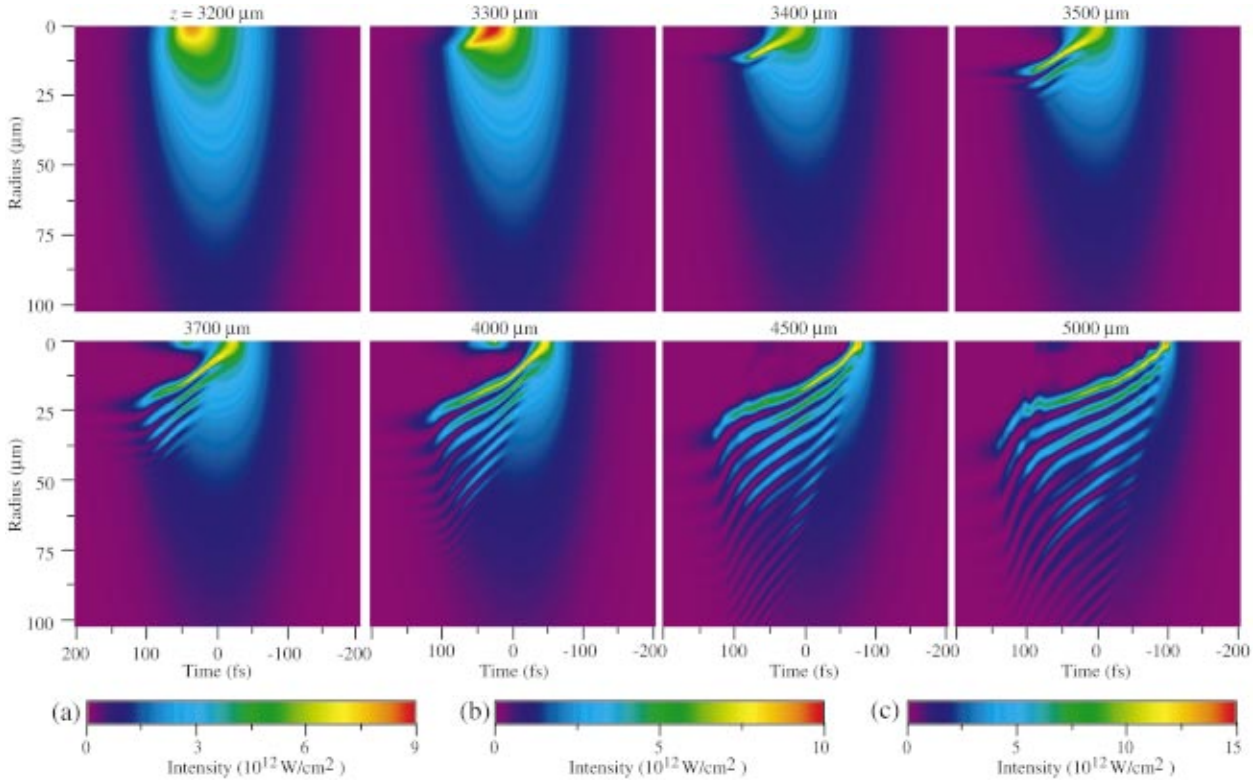

FIG. 2. (Color) Spatiotemporal intensity distribution of an initially Gaussian pulse with an energy of 135 μJ propagating in silica at eight different propagation distances z indicated above each image. The scale of vertical and horizontal axes is common for all the images. The color palette (a) of intensity applies for $z=3200$ μm, (b) for $z=3300$ μm, and (c) for the other values of z. The simulation parameters are indicated in Table I(f). Note that the distribution is cylindrically symmetric around the beam axis $r=0$.

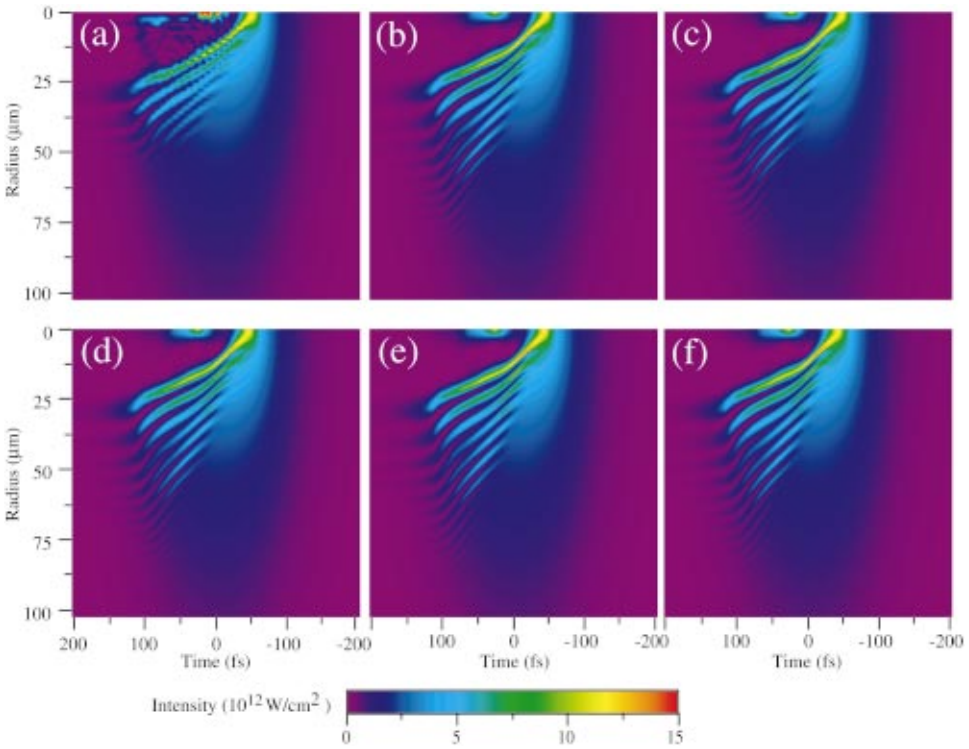

FIG. 3. (Color) Spatiotemporal intensity distribution of an initially Gaussian pulse with an energy of 135 μJ propagating in silica at a propagation distance $z=4000$ μm, calculated with different sets of simulation parameters listed in Table I.

TABLE I. Simulation parameters used for each result in Fig. 3. Δt, Δr, and Δz denote grid spacings in t, r, and z directions, respectively. The ranges of t grids and r grids are $-t_{max}/2<t<t_{max}/2$ and $0<r<r_{max}$, respectively. The rightmost column indicates whether the mask function is set at the r boundary or not.

	Δt (fs)	Δr (μm)	t_{max} (fs)	r_{max} (μm)	Δz (μm)	Absorbing boundary
(a)	4	1.56	1024	400	4	Yes
(b)	2	0.781	1024	400	1	Yes
(c)	2	0.781	2048	800	1	Yes
(d)	2	0.781	1024	400	1	No
(e)	1	0.391	1024	400	1	Yes
(f)	0.5	0.391	1024	400	0.25	Yes

What follows, however, is a dramatic new feature that emerges only when P exceeds P_{cr} by orders of magnitude. A second cone has been formed outside the first cone at $z=3500$ μm. With pulse propagation, more and more cones are formed, resulting in the formation of multiple-cone-like structure by $z=4000$ μm. This structure is formed rapidly during a short interval of several hundreds of μm and propagates stably at least for 2 mm, or over five times Rayleigh length, $z_R=3.6\times10^2$ μm. The time scale of each cone is 15–25 fs, which can still be treated with the SVEA with correction terms. The intensity achieved is at most 1.5×10^{13} W/cm^2, and the maximum value of the fluence is 0.9 J/cm^2. This is smaller than the experimentally obtained threshold fluence for optical breakdown (3–4 J/cm^2) for a 100-fs pulse [18].

As is already mentioned, we have verified the numerical accuracy of our results by changing simulation parameters such as Δr, Δt, Δz, r_{max}, t_{max}, successively. In Fig. 3 we show the spatiotemporal laser intensity profile at $z=4000$ μm calculated with different values of the parameter set, detailed in Table I for the same input energy (135 μJ) as in Fig. 2. The simulation results converge when we use finer grids, i.e., decrease the values of Δt, Δr, and Δz; the grid spacings $\Delta t=2$ fs, $\Delta r=0.781$ μm, and $\Delta z=1$ μm, represented as (b) in Table I are sufficient. While the grid spacings are common for Figs. 3(b)–3(d), the grid size for Fig. 3(c) is twice as large, both in t and r, and the mask function is not set at the r boundary in the case of Fig. 3(d). These three panels are virtually identical, indicating that the reflection of the pulse from the calculation boundary is negligible.

In Fig. 4, we show the variation of the energy contained in the pulse that is absorbed through multiphoton band-to-band transition, and their sum (the total energy), with the propagation distance z for the case of Fig. 2. The total energy is well conserved during the course of the simulation. The constancy of the energy absorption rate at $z>3800$ μm is remarkable. This observation reflects the stability of the multiple-cone structure as can be seen from Fig. 2.

Figure 5 illustrates how the spatiotemporal intensity distribution evolves, when the silica surface is located at $z=2.5$ mm instead of $z=0$ mm. We note that the initial stage of cone formation, in particular, is quite different from that in Fig. 2. This might reflect the fact that self-focusing is sensitive to the interface position. On the other hand, the intensity distribution is less distinctive at later stage.

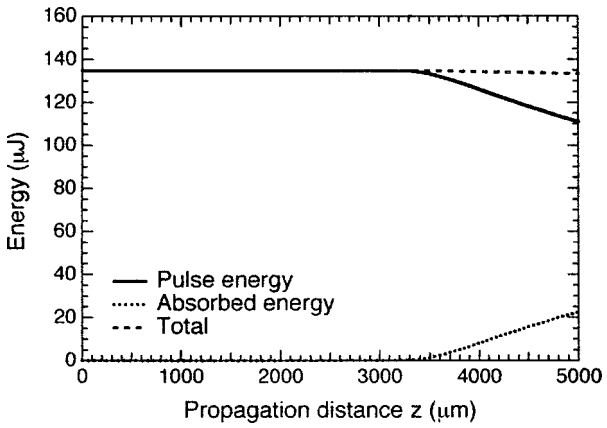

FIG. 4. Variation of the energy contained in the pulse (solid line), the energy absorbed through multiphoton band-to-band transition (dotted line), and their sum (dashed line), with the propagation distance z for the case of Fig. 2.

Figure 6 shows the spatiotemporal intensity distribution for the pulses with an incident energy of 15 and 45 μJ at the propagation distance, at which the multiple-cone formation is nearly saturated. With decreasing pulse energy, the number of cones decreases, and the cones are more parallel to the propagation direction. Though not shown in Fig. 6, the multiple-cone formation ceases when we further decrease the incident pulse energy.

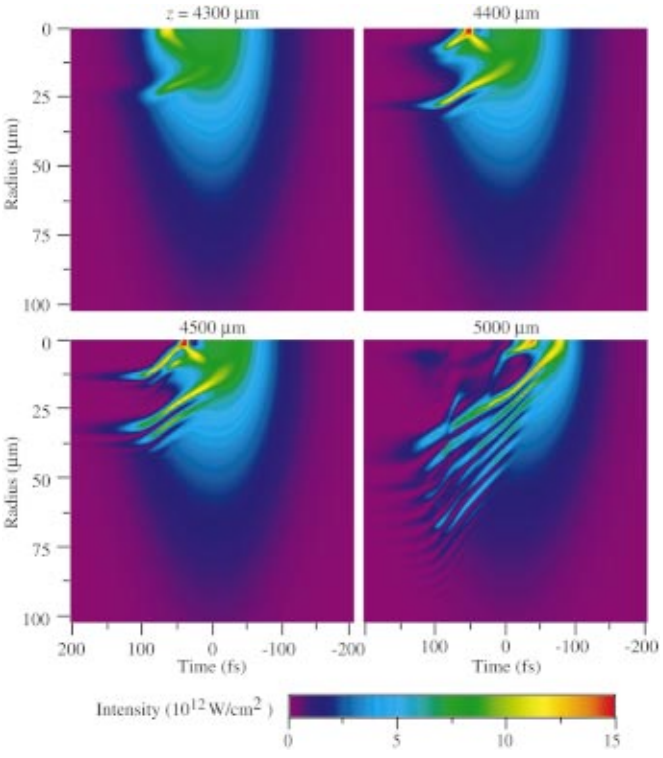

FIG. 5. (Color) Spatiotemporal intensity distribution of an initially Gaussian pulse with an energy of 135 μJ propagating in silica at four different propagation distances z indicated above each image, in cases where the incident surface is located at $z=2.5$ mm.

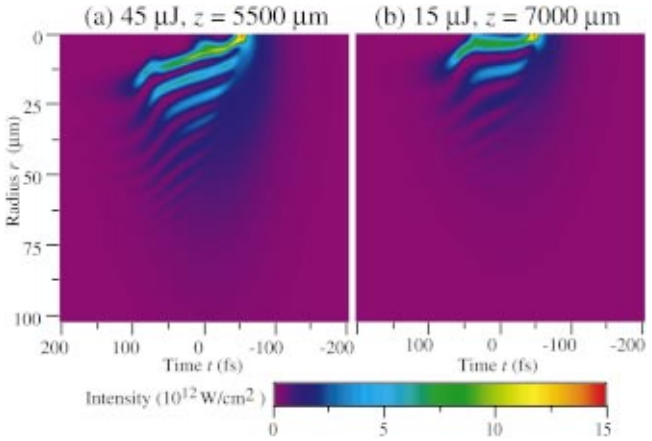

FIG. 6. (Color) Spatiotemporal intensity distribution of an initially Gaussian pulse (a) with an energy of 45 μJ at the propagation distance $z=5500$ μm and (b) with an energy of 15 μJ at $z=7000$ μm. The simulation parameters are indicated in Table I(b).

B. Mechanism of the multiple-cone formation

To explore the mechanism of the multiple-cone formation, in Fig. 7, we show the lateral distribution of the laser-induced refractive index change Δn given by

$$\Delta n = n_2|E|^2 - \frac{1}{2}\frac{\rho}{\rho_{cr}}, \tag{3}$$

at $t=44$ fs and $z=3340$ and 3360 μm, as well as the corresponding intensity distribution. It follows from Eq. (3) that the increase in intensity has a positive contribution, and the increase in conduction electron density, i.e., plasma formation has a negative contribution. In Fig. 7, at $z=3340$ μm, the maximum in Δn is slightly outside the intensity maximum (i.e., the first cone), and Δn is nearly flat in the range $r=9-12$ μm, while the intensity gradually decreases with increasing r. These are because the electron density is higher for smaller value of r. At $z=3360$ μm, the self-focusing is so strong that the first intensity peak takes up much energy from its vicinity. As a result, the peak becomes more prominent and a second local maximum in Δn is formed around $r=11.3$ μm. Once the second peak is formed, the local self-focusing effect leads to the growth of the second cone and to the formation of a third maximum in Δn. The avalanche of this process continues as long as the part of the pulse outside the outermost cone contains sufficient power.

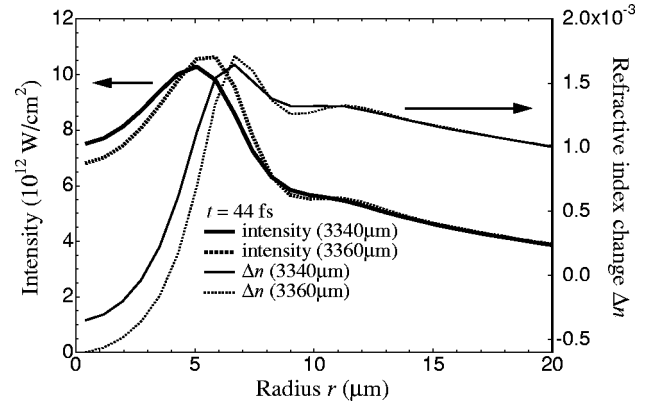

FIG. 7. Radial distribution of intensity (thick lines, left axis) and refractive index change Δn (thin lines, right axis) at $t=44$ fs for the case of Fig. 2. Solid lines are for the propagation distance $z=3340$ μm and dotted lines for $z=3360$ μm.

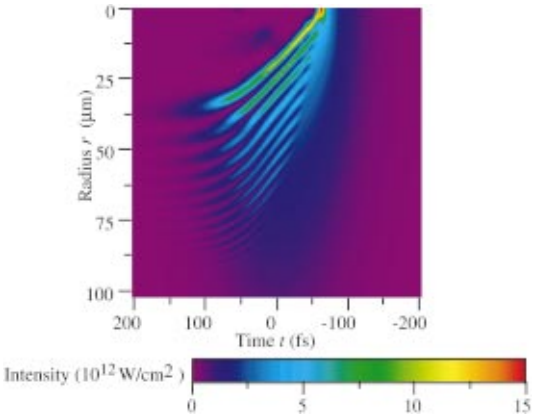

FIG. 8. (Color) Spatiotemporal intensity distribution of an initially Gaussian pulse with an energy of 135 μJ at $z=4000$ μm, calculated by neglecting the dispersion and the terms containing $(i/\omega_0)(\partial/\partial t)$ in Eq. (1). The simulation parameters are indicated in Table I(b).

Figure 8 shows the spatiotemporal intensity distribution at $z=4000$ μm for an input energy of 135 μJ calculated by neglecting the dispersion and the terms containing $(i/\omega_0)\times(\partial/\partial t)$ in Eq. (1). We can see that the intensity distribution exhibits features essentially similar to those in Fig. 2, though quantitative details are different due to the neglect of several terms. This observation confirms that the saturation of the Kerr self-focusing is caused by plasma formation and that the multiple-cone structure is formed by the interplay of the Kerr self-focusing and the plasma defocusing.

C. Effect of the saturation of the conduction electron drift velocity

In Eq. (1), we have assumed a free-electron-like response of conduction electrons in silica. To our knowledge, no quantitative data are available on their response to intense laser fields. The electron drift velocity in a static electric field is proportional to the field up to 2×10^5 V/cm, with a mobility of 21 cm^2/V s [23], and much larger than the maximum velocity of a free electron oscillating in a laser field with the same strength. On the other hand, when the field is higher than a few MV/cm, the drift velocity is saturated at about 2×10^7 cm/s [23], i.e., the maximum free-electron velocity in a laser field with an intensity of $I_{th}=10^{12}$ W/cm^2. Above this intensity, the response of conduction electrons might be significantly different from that of free electrons. To examine the impact of this effect, we have performed simulations by replacing ρ/ρ_{cr} in Eq. (1) with $(\rho/\rho_{cr})f(|E|)$, where

$$f(|E|) = \frac{1}{\sqrt{1+|E|^2/I_{th}}}, \tag{4}$$

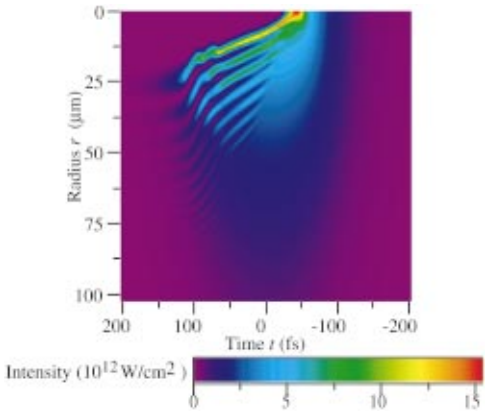

FIG. 9. (Color) Spatiotemporal intensity distribution of an initially Gaussian pulse with an energy of 135 μJ at the propagation distance $z=4000$ μm obtained by taking account of the saturation of conduction electron drift velocity. The simulation parameters are indicated in Table I(b).

models the saturation of electron drift velocity in a simple manner. In Fig. 9, we show the obtained intensity distribution at $z=4000$ μm for the input energy of 135 μJ. Although the cones are shifted toward the beam axis due to smaller plasma defocusing, the image is similar to the corresponding one in Fig. 2.

D. Photoionization rate

Among the material parameters used in the present study, the photoionization rate is the most uncertain. The Keldysh theory may underestimate or overestimate the multiphoton ionization cross section even by six orders of magnitude. We have examined how the error in σ_6 affects our results by simulating the pulse propagation, by varying the value of σ_6 from 2.6×10^{-182} $s^5\,cm^{12}$ to 2.6×10^{-174} $s^5\,cm^{12}$, i.e., from 10^{-2}–10^6 times the value used for the case of Fig. 2. The results are shown in Fig. 10. The multiple-cone formation can be seen for a very wide range, over six orders of magnitude (2.6×10^{-182} $s^5\,cm^{12}$ to 2.6×10^{-176} $s^5\,cm^{12}$) of σ_6, though its quantitative details depend on σ_6: the maximum intensity and the number of cones decrease, and the size of each cone becomes larger with an increasing value of σ_6. Although multiple cones are not formed in the case of $\sigma_6=2.6\times10^{-174}$ $s^5\,cm^{12}$ [Fig. 10(d)], the possibility of so high a value of σ_6 might be excluded on the basis of an unplausibly low maximum intensity achieved ($\sim7\times10^{11}$ W/cm^2). The surprising robustness against the error in σ_6 is explained as follows: from the viewpoint of the band-to-band transition rate in Eq. (2), the decrease in σ_6 by two orders of magnitude is recovered by the increase in intensity only by $\sqrt[6]{100}=2.2$. This does not affect the propagation behavior significantly. As can be expected from this argument, the maximum intensity increases gradually with

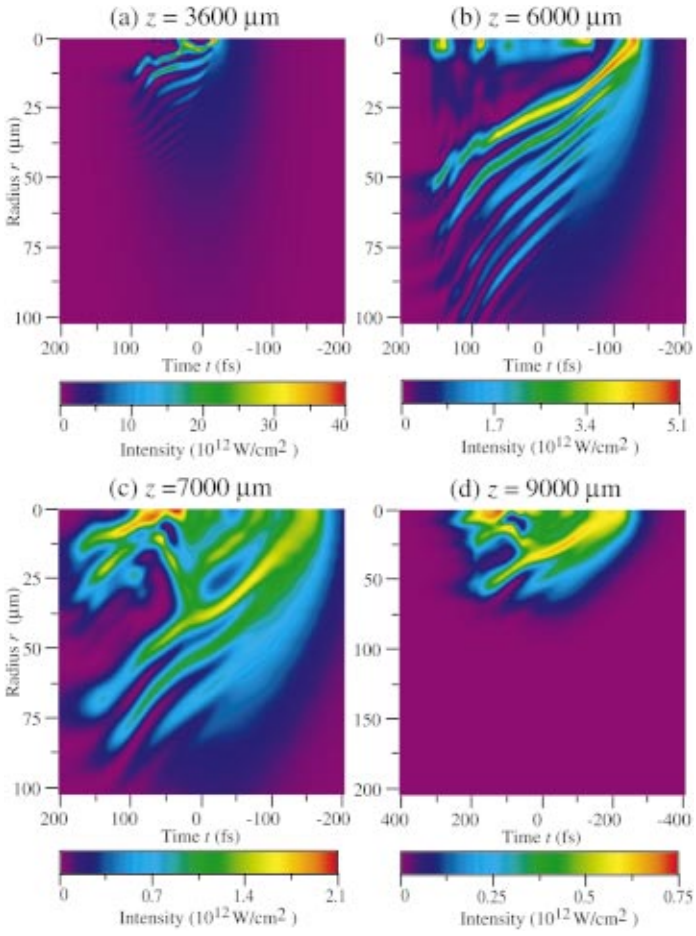

FIG. 10. (Color) Spatiotemporal intensity distribution of an initially Gaussian pulse with an energy of 135 μJ at a propagation distance z indicated above each image, obtained with a value of σ_6, which is (a) 10^{-2}, (b) 10^2, (c) 10^4, (d) 10^6 times as large as for Fig. 2. The simulation parameters are indicated in Table I(b).

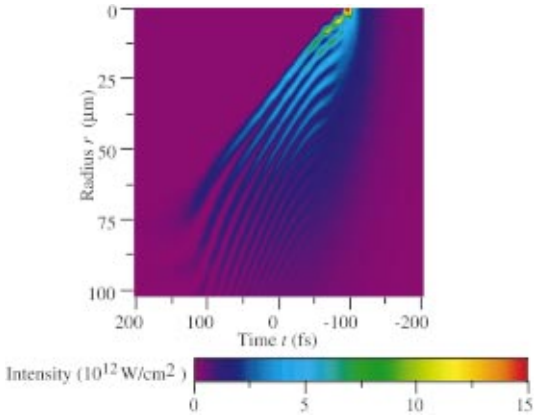

FIG. 11. (Color) Spatiotemporal intensity distribution of an initially Gaussian pulse with an energy of 135 μJ at the propagation distance $z=5000$ μm obtained by taking account of the avalanche ionization based on Thornber's model [Eq. (5)]. The simulation parameters are indicated in Table I(b).

decreasing multiphoton ionization cross section σ_6. While it is difficult to obtain results for σ_6 smaller than 2.6×10^{-182} s^5 cm^{12}, since our simulation code is not stable for such a range of σ_6, the maximum fluence is expected to reach the damage threshold ($3-4$ J/cm^2 [18]).

In Eq. (2) we have assumed that multiphoton ionization dominates over avalanche ionization. However, the latter may not be completely negligible, even in case of 130-fs pulses. If we include avalanche ionization, Eq. (2) is replaced by

$$\frac{\partial\rho}{\partial t}=\eta(|E|)\rho+\sigma_6\left(\frac{|E|^2}{\hbar\omega_0}\right)^6(\rho_0-\rho), \tag{5}$$

where $\eta(|E|)$ denotes the electron avalanche rate, which can be expressed, according to Thornber's model [14], as

$$\eta(E)=\frac{v_s eE}{U_i}\exp\left(-\frac{E_i}{E(1+E/E_p)+E_{kT}}\right), \tag{6}$$

where U_i denotes the band gap energy, v_s is the saturation conduction electron drift velocity, and E_{kT}, E_p, and E_i are threshold fields for electrons to overcome the decelerating effects of thermal, phonon, and ionization scattering, respectively. In order to obtain an insight of the impact of avalanche ionization, we have performed simulations with Eq. (5) instead of Eq. (2) and with the correspondingly modified version of Eq. (1). The following values of the parameters in Eq. (5) are used: $U_i=9.0$ eV, $v_s=2\times10^7$ cm/s [23], $E_{kT}=3.6\sqrt{\mathrm{W/cm^2}}$, $E_p=1.2\times10^5\sqrt{\mathrm{W/cm^2}}$, and $E_i=1.1\times10^6\sqrt{\mathrm{W/cm^2}}$ [19]. The spatiotemporal intensity distribution at $z=5000$ μm obtained for an input energy of 135 μJ is shown in Fig. 11. We can again see that the laser pulse is transformed into multiple cones. The angle between the cones and the propagation axis is larger than in Fig. 2. This is because avalanche ionization promotes the plasma production at the trailing edge of the pulse, leading to stronger defocusing there.

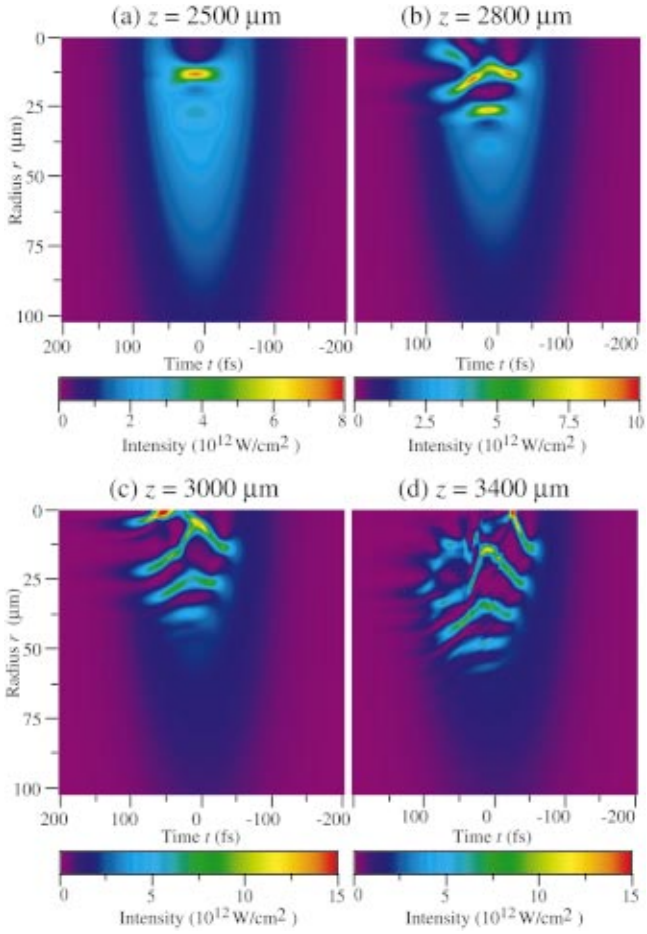

FIG. 12. (Color) Spatiotemporal intensity distribution of a pulse with an incident energy of 135 μJ at four different propagation distances z indicated above each image. The initial radial profile of the pulse is Gaussian, slightly modulated by an oscillating function Eq. (7) with $a=10^{-3}$ and $\Lambda=100$ μm. The simulation parameters are $\Delta t=0.5$ fs, $\Delta r=0.781$ μm, $\Delta z=0.5$ μm, $t_{\max}=1024$ fs, and $r_{\max}=400$ μm.

Strictly speaking, Thornber's model of avalanche ionization [Eq. (5)] [14] may not be applied in the fs-pulse regime [16,17]. Moreover, tunneling ionization may dominate over multiphoton ionization at the highest intensity achieved. Anyway, the Keldysh theory may deviate largely from real photoionization rates. It follows, however, from the preceding discussion that the multiple-cone formation is a robust phenomenon, whose qualitative nature does not depend on the details of the response and the production rate of conduction electrons, as long as the photoionization rate rapidly increases with intensity. It is expected, therefore, that the essence of our results, especially the multiple-cone formation, may hold for many other solids and liquids. Now we can divide the fs-pulse propagation without breakdown, into three different power regimes. In the low-power regime ($P<P_{cr}$), the propagation is predominantly linear. In the intermediate regime ($P\approx$ several times P_{cr}), the filamentation and the temporal splitting is observed. In the high-power regime ($P\approx$ several tens to hundreds of times P_{cr}), the multiple-cone structure is formed.

E. Modulation instability

In the present study we assume that the input pulse is an unperturbed Gaussian beam. It is known, however, that inhomogeneity may lead to a breakup of the beam into several filaments [6]. In order to get an insight of how the multiple-cone formation is affected by this modulation instability, we have performed simulations, in which the electric field amplitude of the input pulse is that of a Gaussian beam slightly modulated by an oscillating function,

$$f_{\mathrm{mod}}(r) = 1 + a \sin\frac{2\pi r}{\Lambda}, \tag{7}$$

where a and Λ are constant parameters. Figure 12 shows the evolution of the pulse in the case of $a = 10^{-3}$ and $\Lambda = 100\ \mu$m. In the presence of the modulation, the beam does not evolve as a single hump, but it is transformed into a double ring around the propagation axis [Fig. 12(a)]. Then, while the middle part of the rings tend to merge again [Fig. 12(b)], the posterior and the peripheral parts of the pulse form a structure similar to multiple cones [Figs. 12(c) and 12(d)]. Thus, the feature of the multiple-cone formation is still present, though perturbed by modulation instability.

In order to take the effect of azimuthal inhomogeneity into account, we must resort to fully three-dimensional simulations [3] instead of the axially symmetric modeling. While this has not been done in the present study, mainly due to the constraint of computational time, the competition of the multiple-cone formation and the modulation instability in fully three-dimensional situations should be investigated in future work.

IV. CONCLUSIONS

We have presented numerical simulations of the Gaussian fs-pulse propagation in silica in the high-power regime, where the power of the incident pulse is from several tens to several hundreds of times higher than P_{cr} of the solid. Our results have revealed that the pulse is split many times, both temporally and spatially and that, as a result, the intensity distribution contains multiple cones, which are not parallel to the propagation axis, though they are nearly parallel to each other. The cones are formed rapidly within several 100 μm by the interplay of Kerr self-focusing and plasma defocusing. As the input pulse energy increases from 15 μJ to 135 μJ, the angle between the cones and the propagation axis, and the number of the formed cones also increase.

The account of the drift velocity saturation of conduction electrons, the uncertainty of the band-to-band transition rate, and the modulation instability do not influence the essence of our results much; the multiple-cone structure is formed in any case, though its quantitative details are affected. This observation strongly supports the physical reality of this feature.

ACKNOWLEDGMENT

This work was supported by the Special Postdoctoral Researchers Program of RIKEN.

[1] J.E. Rothenberg, Opt. Lett. **17**, 1340 (1992).
[2] M. Mlejnek, E.M. Wright, and J.V. Moloney, Phys. Rev. E **58**, 4903 (1998).
[3] M. Mlejnek, M. Kolesik, J.V. Moloney, and E.M. Wright, Phys. Rev. Lett. **83**, 2938 (1999).
[4] J.K. Ranka and A.L. Gaeta, Opt. Lett. **23**, 534 (1998).
[5] L. Bergé and A. Couairon, Phys. Rev. Lett. **86**, 1003 (2001).
[6] S. Tzortzakis *et al.*, Phys. Rev. Lett. **86**, 5470 (2001).
[7] N. Aközbek, M. Scalora, C.M. Bowden, and S.L. Chin, Opt. Commun. **191**, 353 (2001), and references therein.
[8] I.P. Christov, H.C. Kapteyn, M.M. Murname, C.-P. Huang, and J. Zhou, Opt. Lett. **20**, 309 (1995).
[9] A.A. Zozulya, S.A. Diddams, A.G. Van Engen, and T.S. Clement, Phys. Rev. Lett. **82**, 1430 (1999).
[10] J.K. Ranka, R.W. Schirmer, and A.L. Gaeta, Phys. Rev. Lett. **77**, 3783 (1996).
[11] S. Tzortzakis *et al.*, Phys. Rev. Lett. **87**, 213902 (2001).
[12] H. Kumagai, S.-H. Cho, K. Ishikawa, and K. Midorikawa, J. Opt. Soc. Am. B (to be published).
[13] L.V. Keldysh, Zh. Eksp. Teor. Fix. **47**, 1945 (1964) [Sov. Phys. JETP **20**, 1307 (1965)].
[14] K.K. Thornber, J. Appl. Phys. **52**, 279 (1981).
[15] F. Docchio, P. Regondi, M.R.C. Capon, and J. Mellerio, Appl. Opt. **27**, 3661 (1988).
[16] J. Noack and A. Vogel, IEEE J. Quantum Electron. **35**, 1156 (1999).
[17] C.-H. Fan and J.P. Longtin, Appl. Opt. **40**, 3124 (2001).
[18] A.-C. Tien, S. Backus, H. Kapteyn, M. Murnane, and G. Mourou, Phys. Rev. Lett. **82**, 3883 (1999).
[19] D. Du, X. Liu, G. Korn, J. Squier, and G. Mourou, Appl. Phys. Lett. **64**, 3071 (1994).
[20] G.P. Agrawal, *Nonlinear Fiber Optics*, 2nd ed. (Academic, San Diego, 1995).
[21] S.E. Koonin *et al.*, Phys. Rev. C **15**, 1359 (1977).
[22] J.L. Krause, K.J. Schafer, and K.C. Kulander, Phys. Rev. A **45**, 4998 (1992).
[23] R.C. Hughes, Solid-State Electron. **21**, 251 (1978).